ORIGINAL ARTICLE

The effect of transition metal oxides in the La/TiO$_2$ structure for the photocatalytic degradation of malachite green under UV and visible light irradiation

Nastaran Parsafard[1] · Zahra Shoorgashti[1]

Abstract

Herein, La@M$_x$O$_y$/TiO$_2$ (M = V, Cr, Mn and Fe) composite catalysts were prepared based on the sol–gel method as an effective adsorbent and photocatalyst for the degradation of malachite green from an aqueous solution under UV–Vis light. Under experimental conditions, a maximum adsorption capacity of 57.10% for the malachite green dye was achieved with La@Fe$_2$O$_3$/TiO$_2$. Moreover, this composite showed 78.62% photodegradation efficiency for malachite green. A quadratic model constructed using the response surface method showed that the maximum efficiency of photodegradation of malachite green can be achieved at pH 11 and a process time of 35 min.

Keywords Malachite green · Sol–gel method · Photodegradation · UV–Vis light · Response surface methodology · Efficiency

Introduction

Dyes are among the environmental pollutants that have the most negative impact on surface and groundwater (Jaffari et al. 2023). Malachite green (MG) is one of the most commonly used dyes in the textile, leather, printing and food industries with high water solubility, causing teratogenic, carcinogenic and reproductive abnormalities in animals and humans (Sharma et al. 2023). There are various chemical, physical and biological methods to treat water contaminated with MG and remove it as a pollutant (Sharma et al. 2023; Chakraborty et al. 2022; Hojjati-Najafabadi et al. 2023; Tran et al. 2022; Verma et al. 2020; Khurshid et al. 2021). Among these methods, photodegradation of MG has received more attention in recent decades because this method is environmentally friendly highly efficient and cost-effective, does not cause secondary pollution and has fewer drawbacks and limitations (Jaffari et al. 2023; Sharma et al. 2023).

Photocatalysts can be a promising choice to complete the removal of dyes due to redox conversion and to decompose dyes (Rauf et al. 2011). Among the many catalytic supports reported for this method, titanium dioxide has attracted the most attention due to its attractive electro-optical properties, cheapness, chemical stability and non-toxicity (Rauf et al. 2011; Balakrishnan et al. 2022).

To improve the photocatalytic properties of titanium dioxide, researchers have focused on the use of composite catalysts for the photodegradation of dyes in recent years. For example, Zhang et al. prepared and used multi-walled carbon nanotubes with titanium dioxide as a composite catalyst for the photodegradation of malachite green. This catalyst was loaded with different concentrations of cobalt solution. They obtained reasonable photocatalytic efficiency of Co@CNT/TiO$_2$ composites compared to the individual components of this catalyst (Zhang et al. 2024).

Kallawar et al. prepared Bi@TiO$_2$/reduced graphene oxide (rGO) nanocomposites with different loadings of bismuth (Bi) using a sol–gel method assisted by ultrasonic waves for the photodegradation of malachite green under visible light. The reported degradation for this catalyst was 93.34% under the optimum conditions used (Kallawar et al. 2023).

Another researcher, Yulizar and coworkers, modified titanium dioxide with yttrium manganite (YMnO$_3$) and achieved a MG photodegradation efficiency of 95.34% under visible light with this new catalyst (Yulizar et al. 2023).

✉ Nastaran Parsafard
  n-parsafard@kub.ac.ir

1   Department of Applied Chemistry, Kosar University
    of Bojnord, North Khorasan, Iran

In 2022, a sulfur-doped titanium dioxide/porous reduced graphene oxide catalyst was prepared by Giang et al. and used to remove malachite green under UV and visible light. In this work, S-TiO$_2$ was prepared by the sol–gel method with different calcination temperatures, and the S-TiO$_2$/rGO catalyst was synthesized by the in situ method using hydrothermal and ultrasonic methods. The results show that the S-TiO$_2$/rGO catalyst exhibits 99.86% MG photodegradation efficiency, which is higher than that of S-TiO$_2$ (78.88%) (Giang et al. 2022).

In addition, Bibi and coworkers have shown that titanium in a nanocomposite structure of rGO-Fe$_3$O$_4$/TiO$_2$ exhibits better photodegradation of MG (99%) under visible light at a process time of 55 min (Bibi et al. 2021).

On this basis, various methods have been used to increase the photocatalytic activity of TiO$_2$. Among the various materials used for this purpose, transition metal oxides are interesting promoters for the photocatalytic degradation of dyes. A number of works have reported the ability of transition metal oxides to improve the surface or bulk properties of semiconductor catalysts (Wu et al. 2012; Pei and Woon 2013; Lam et al. 2014a). Lam et al. used three different transition metal oxides such as WO$_3$, CuO and NiO in the structure of ZnO nanorods for the photodegradation of phenol under UV–Vis irradiation (Lam et al. 2014b).

According to the research reports, iron oxide (Fe$_2$O$_3$) and manganese dioxide (MnO$_2$) are suitable candidates of transition metal oxides as semiconductors (Warsi et al. 2021).

To investigate the enhancing effect of transition metal oxides on the photocatalytic properties of TiO$_2$ and the change in this performance in one period of the periodic table, a composite catalyst of metal oxides such as vanadium, chromium, manganese and iron with titanium dioxide was prepared. To improve the performance, lanthanum was impregnated on these catalysts. In this work, the photocatalytic activities of the prepared catalysts and their structural properties were investigated by characterization analyses such as X-ray diffraction (XRD), Fourier transform infrared spectroscopy (FTIR), UV–Vis diffuse reflectance spectroscopy (UV–Vis DRS), N$_2$ adsorption–desorption analysis and scanning electron microscopy (SEM). In addition, the dependence of the photocatalytic performance in the degradation of malachite green on the pH value was also investigated in the present work. These parameters as independent factors were also investigated using response surface methodology (RSM) to optimize their effects on the photodegradation efficiency of malachite green.

Materials and methods

Catalyst preparation

The iron oxide (Fe$_2$O$_3$) and manganese oxide (MnO$_2$) were synthesized according to the method described by Warsi et al. (Warsi et al. 2021). To synthesize Fe$_2$O$_3$, 1 mol of FeCl$_2$ ($m_{FeCl2} = 1.18$ g) and 2 mol of FeCl$_3$ ($m_{FeCl3} = 1.52$ g) were separately mixed with hydrochloric acid ($m_{HCl} = 0.68$ g). Then, these two solutions were stirred together. After gradual addition of the ammonia solution ($m_{NH3} = 0.21$ g) with stirring for 2.5 h, a brown solid was obtained, which reached a pH of 9.8. This solid was washed and dried overnight at 70 °C.

To produce MnO$_2$, potassium permanganate ($m_{KMnO4} = 1.82$ g) reacted with fumaric acid ($m_{C4H4O4} = 2.00$ g) in an oxidation–reduction reaction. Sulfuric acid (2.5 M) and deionized water were added to this solution. The pH of the solution was kept constant at 5. This solution was dried at 100 °C and calcined at 450 °C for 5 h. The disappearance of the violet color of the solution indicates the end of the reaction and the depletion of the available potassium permanganate.

Cr$_2$O$_3$ was synthesized according to the method described by Almontasser and Parveen (Almontasser and Parveen 2020). In this method, chromium (III) nitrate nonahydrate (Cr(NO$_3$)$_3$.9H$_2$O) was used as a precursor. For this purpose, two separate aqueous solutions of this compound ($m_{Cr(NO3)3} = 5.27$ g) and sodium hydroxide ($m_{NaOH} = 1.58$ g) were prepared. These two solutions were mixed together and stirred at 40 °C for 20 min. Then, the temperature was raised to 80 °C for 2 h while the solution was stirred and sealed in a container. The resulting dark green gel was dried at 100 °C first on a heater, then in an oven for 3 days and finally in a furnace at a temperature of 500 °C for 3 h.

The following method (Farahmandjou and Abaeiyan 2017) was used to synthesize the V$_2$O$_5$ powder. An aqueous solution of sodium meta-vanadate (as a precursor, $m_{V2O5} = 1.34$ g) was prepared with stirring at room temperature. Then, ammonium chloride ($m_{NH4Cl} = 0.59$ g) was added to this solution until it dissolved completely. After 10 min, cetyl trimethyl ammonium bromide (CTAB, $m_{CTAB} = 0.40$ g) was dissolved in this solution at 80 °C. During the reaction, the color of the solution fluctuated from orange to light yellow, and the pH of the solution changed between 6 and 8. The resulting solution was evaporated for 2 h, and the subsequent solid was calcined at 500 °C for 5 h.

To synthesize the composite catalysts from TiO$_2$ and transition metal oxides, the sol–gel method (Abbas et al. 2016) was used. First, each transition metal oxide (1 g) was added to deionized water and stirred at room temperature. This solution was added to the TiOCl$_2$ solution (1 M) and stirred for 30 min. The final pH should be 9. The resulting solution was aged at 80 °C for 4 h and then stirred again for 12 h. The solid obtained was filtered, washed and dried in an oven at 80 °C overnight. Finally, the powdered products were calcined at 600 °C for 2 h.

La-doped composite catalysts were synthesized using the impregnation method. Lanthanum nitrate hexahydrate

($La(NO_3)_3.6H_2O$) as a precursor of La was dissolved in ethanol to obtain an adjusted molar concentration (1 wt%, $V_{La(NO3)3} = 1.27$ ml). This solution was added dropwise to the aqueous mixture of each composite catalyst with stirring at room temperature for 2 h. The resulting solution was stirred at 60 °C for 2 h. Subsequently, the powder solid was dried in an oven at 110 °C overnight. Finally, the obtained La-supported catalysts were calcined at 300 °C for 4 h. The obtained catalysts, La/TiO_2-V_2O_3, La/TiO_2-Cr_2O_3, La/TiO_2-MnO_2 and La/TiO_2-Fe_2O_3, were named as LTV, LTC, LTM and LTF, respectively.

The characterization of composite catalysts

The specification of the structure and other properties of the produced catalyst oxide nanoparticles were carried out by various analyses. The following is a summary of the methods used:

X-ray diffraction (XRD) patterns were recorded with an X-ray diffractometer (XRD Philips PW1730) using Cu K_α radiation to study the crystal phase of each catalyst. The X-ray fluorescence (XRF) analysis on all prepared catalyst samples to measure the exact amount of lanthanum incorporated by using XRF Philips PW2404.

Fourier transform infrared spectroscopy (FTIR) was used to understand the chemical bonding. The FTIR spectra were recorded using a Nicolet™ iS™ 10 FTIR spectrometer in the wavenumber range of 400–4000 cm^{-1}.

UV–Vis/diffuse reflectance spectroscopy (UV–Vis/DRS) was performed using an Evolution 300 UV–Vis spectrophotometer.

Scanning electron microscopy (SEM) images were taken with a SEM VEGA3. N_2 adsorption–desorption isotherms were generated using a BET BELSORP Mini II to characterize the surface areas and porosity.

Photocatalytic test

The photocatalytic activity of each composite catalyst was evaluated using 10 ppm aqueous solution of malachite green (MG) under an Hg lamp (500 W) as an ultraviolet (UV) light source and sunlight as a visible (vis) light source. A 0.25 g of each photocatalyst was distributed over 30 ml of a 10 ppm MG solution and stirred in the dark for 60 min to achieve adsorption–desorption equilibrium. The mixture was then irradiated with exposed to UV–Vis light and analyzed at 5-min intervals. The reaction was carried out at three pH values (pH = 3, 7 and 11) for 35 min at 25 °C. The centrifuged samples were then analyzed using a UV–Vis spectrophotometer (Evolution 300).

The photocatalytic activity of each catalyst was measured by the photo-decolorization efficiency (PDE) of MG according to the following equation:

$$PDE(\%) = 1 - \frac{A_t}{A_0} \times 100 \qquad (1)$$

where A_0 is the absorbance of the initial concentration of MG, and A_t is the absorbance of MG concentration at different times under UV–Vis light.

Experimental design and optimization by RSM

The influence of the key factors and achieving optimal points in the photocatalytic degradation efficiency of MG using the prepared catalysts, the experimental data were investigated using Design Expert software, version 11. The two independent factors selected in this work were the pH of MG solution and process time, while the photodegaradation efficiency (PDE) of MG served as the response and dependent variable. The influence of these independent parameters on the PDE was evaluated in 13 series of experiments using a central composite design (CCD).

Results and discussion

Characterization of the synthesized catalysts

Figure 1 shows the FTIR spectra of the composite catalysts. The characteristic peaks of TiO_2 and rutile TiO_2 are observed at 440 cm^{-1} and 656 cm^{-1}, respectively (Zhang et al. 2002). The absorption peaks at about 3400 and 1640 cm^{-1} may indicate the stretching and bending vibrations of the hydroxyl group of water molecules due to the moisture content of the solids. In the LTF spectrum, two bands at 418 and 598 cm^{-1} are assigned to Fe–O vibrations (Fatima et al. 2020).

The spectrum of the LTM catalyst shows two stretching modes of O–Mn–O in the range from 457 to 599 cm^{-1} range (Warsi et al. 2021). Two peaks at 598 and 652 cm^{-1} in the LTC spectrum are also attributed to Cr–O stretching modes (Farzaneh and Najafi 2011). The IR spectrum of LTV shows the bands at 997 and 559 cm^{-1}, which correspond to the V–O stretching vibrations (Farahmandjou and Abaeiyan 2017). According to the available reports, other peaks at 1040, 1310, 1320 and 1440 cm^{-1} could be related to the carbonate species of lanthanum ($La_2O_2CO_3$) (Taylor and Schrader 1991).

Figure 2 shows the UV–Vis/DRS of these composite catalysts. The observed absorption bands at ~280 nm (weak and broad peak) and ~350 nm (highest absorption peak which is characteristic of the rutile phase of TiO_2) in the UV light region correspond to a charge transfer from the oxygen surface to titanium. As can be seen in these spectra, another broad peak can be seen at a wavelength above 450 nm, which can be associated with the interaction of surface

Fig. 1 The FTIR spectra of the composite catalysts
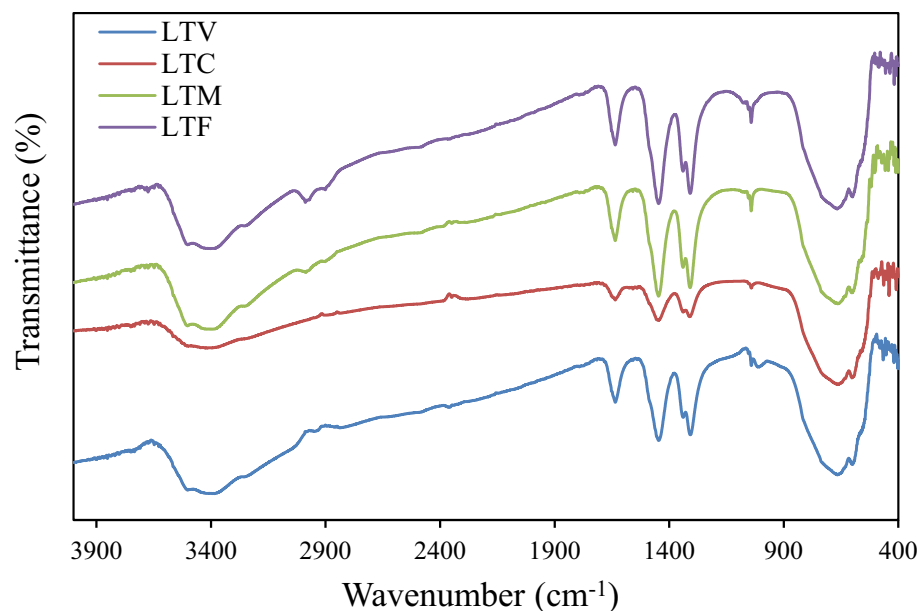
metal oxides with TiO_2 in the composite catalyst (Pan et al. 2020).

The modification of photocatalysts through doping can significantly alter their photoabsorption characteristics, which, in turn, affects their photocatalytic activities.

La doping introduces additional energy levels within the bandgap of TiO_2, which can extend its absorption edge into the visible light region. This phenomenon is often referred to as a "red shift" in the UV–Vis/DRS spectra, indicating enhanced photoabsorption capability under visible light. As demonstrated in the study by Huang et al. (Huang et al. 2017), the UV–Vis DRS spectra of La-doped TiO_2 exhibited

a red shift compared to pure TiO_2, suggesting improved photoabsorption in the visible light region.

Furthermore, La doping can introduce oxygen vacancies and/or surface defects in the TiO_2 lattice, which can enhance the photocatalyst's ability to generate and separate electron–hole pairs. According to Wang et al. (Huang et al. 2017), these defects can reduce the recombination rate of photo-generated electron–hole pairs, leading to higher quantum efficiencies and improved photocatalytic activity under visible light.

Figure 3 shows the SEM images of the La-loaded TiO_2-Fe_2O_3 composite catalyst at different magnifications.

Fig. 2 The UV–Vis/DRS of the composite catalysts
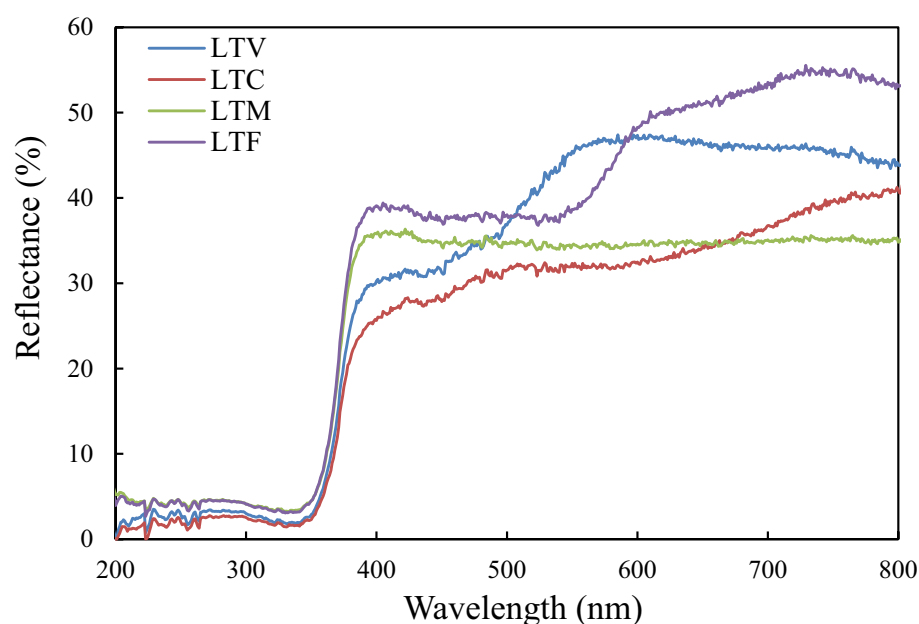
Since other catalysts show similar images, only the morphology of this catalyst was discussed. As can be seen in these images, the Fe_2O_3 content in the TiO_2 matrix affects the morphology of the composites in the form of an irregular structure. The images show spherical particles due to the lanthanum deposited on the surface of the catalysts during the impregnation process.

Our XRF results indicate that the lanthanum content in the catalysts closely matches the intended doping levels, thereby confirming the successful incorporation of lanthanum into the composite structure. The structural properties, including the surface area, total pore volume and average pore diameter of the prepared photocatalysts, are summarized in Table 1. The BET and BJH isotherms are also shown for the LTF catalyst in Fig. 4.

The isotherms of all the prepared catalysts fit well to the type IV isotherm curve and the hysteresis loops are of type H3 according to the IUPAC classification. This result shows that all catalysts have a mesoporous structure with an average pore diameter between 31 and 44 nm (Bootluck et al. 2022). The catalysts LTF, LTM, LTV and LTC each exhibit the good surface area among the catalysts evaluated.

The crystal structure of the prepared composite catalysts was investigated by XRD analysis. Figure 5 shows the XRD patterns of the composite catalysts LTV, LTC, LTM and LTF. The XRD pattern of the LTF composite shows that the peaks at 25.39° (101), 37.89° (112) and 48.19° (200) indicate the presence of the anatase phase, while the peaks

Table 1 Textural and surface properties of the prepared catalysts

Catalysts	Surface area ($m^2\ g^{-1}$)	Total pore volume ($cm^3\ g^{-1}$)	Average pore diameter (nm)
LTV	81.676	0.016	33.471
LTC	79.337	0.015	31.648
LTM	93.805	0.018	37.655
LTF	110.130	0.021	43.931

Fig. 3 The SEM images of the composite catalysts
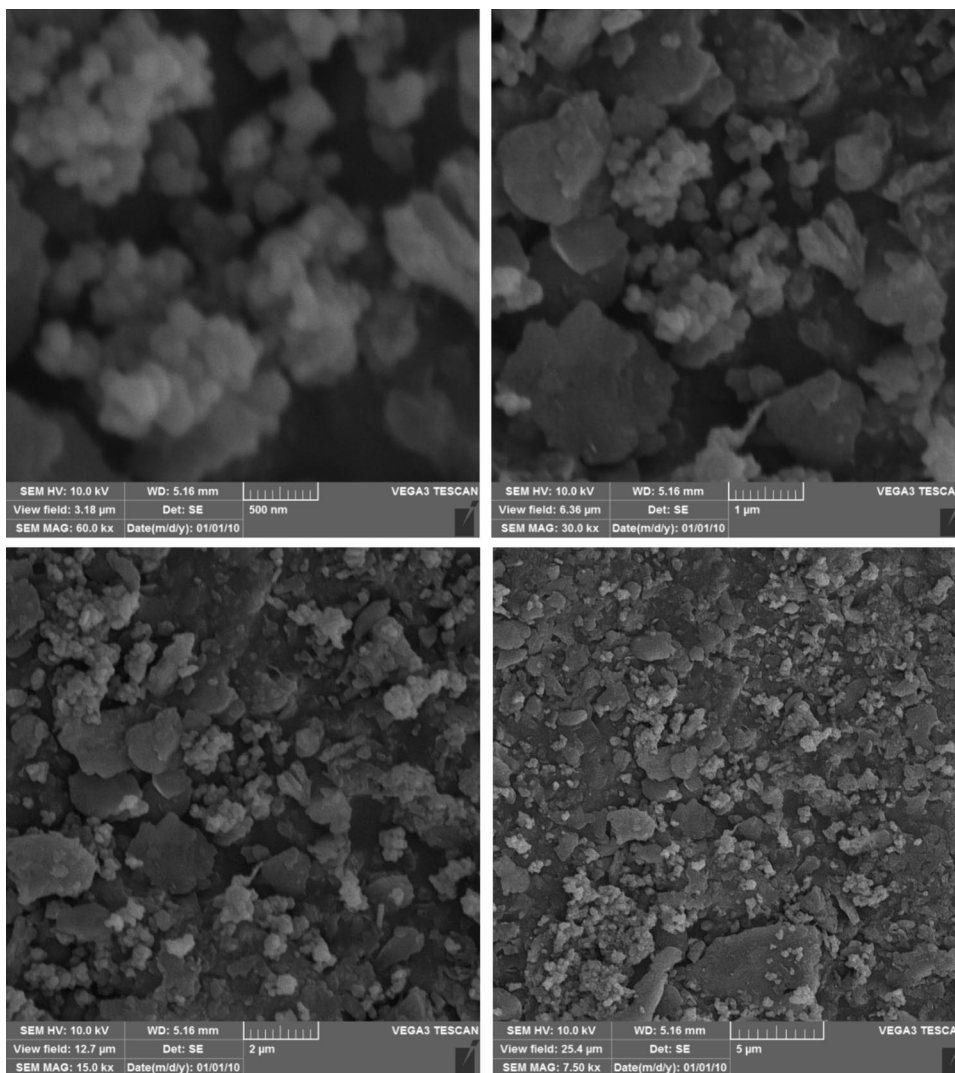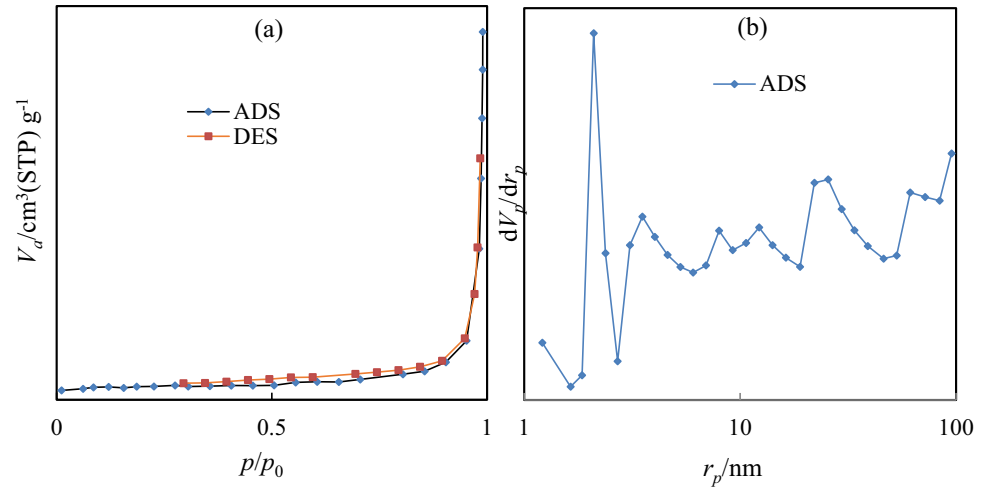
at 27.54° (110), 35.49° (101) and 53.99° (211) indicate the presence of the rutile phase (Abbas et al. 2016).

The average crystallite size of anatase phase (101) can be measured with the Scherrer equation:

$$D = \frac{K\lambda}{\beta \cos\theta} \qquad (2)$$

where D is the average crystallite size, K is a constant (0.89 here), λ is the X-ray wavelength (0.15418 nm), β is the band broadening in radians (full width at half maximum) and θ is the peak position versus Bragg angle. The particle sizes are calculated to be between 17.02 and 21.27 nm.

There are very weak 2θ peaks in these patterns that can be associated with the transition metal oxides in the structure

of the composites. The 2θ peaks at 29.9°, 34.29°, 42.69°, 56.99° and 62.19° are relevant to the (220), (311), (400), (511) and (440) crystal planes of Fe_2O_3 in the LTF catalyst (Abbas et al. 2016).

The diffraction pattern of the LTM catalyst shows the diffraction angles of manganese oxide at 26.04° (220), 28.59° (310), 36.54° (400), 37.54° (211), 42.04° (301), 46.94° (321), 49.79° (411), 52.14° (440), 55.64° (600), 56.49° (501), 60.09° (521), 65.29° (002), 69.54° (541), 72.89° (312), 77.09° (402) and 78.69° (332) (Warsi et al. 2021).

The LTC pattern shows the weak characteristic peaks at 2θ = 24.54°, 33.64°, 36.29°, 39.74°, 41.54°, 44.29°, 50.29°, 54.89°, 58.19°, 63.59°, 72.94° and 77.04°, which reveal the Cr_2O_3 in the LTC composite catalyst (Almontasser and Parveen 2020).

Fig. 5 The XRD patterns of the synthesized catalysts
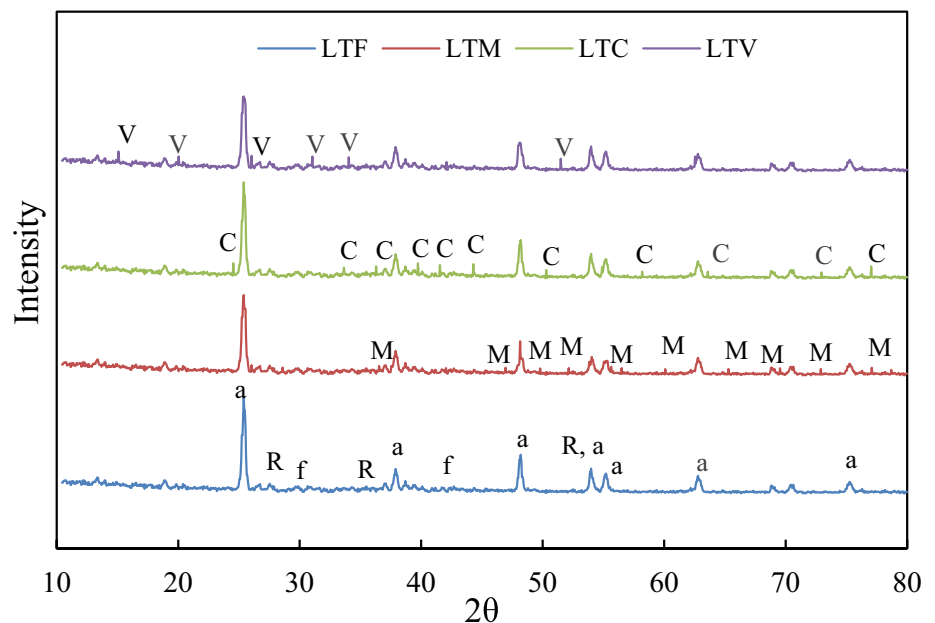
The weak characteristic peaks of V_2O_5 in LTV catalyst were observed at $2\theta = 15.09°$ (200), 20.04° (010), 26.04° (101), 31.04° (310), 34.04° (301), 42.09° (020), 47.99° (600), 51.49° (002) and 62.54° (701) (Farahmandjou and Abaeiyan 2017).

The characteristic diffraction peaks of the lanthanum species in the X-ray diffractions of the prepared catalysts were not observed. This could be due to the fact that the lanthanum species were highly dispersed on the surface of the composite catalysts.

Performance of composite catalysts for the MG degradation

First, the adsorption experiments were evaluated by adding 0.25 g of each composite catalyst to 30 ml of MG solution at a concentration of 10 ppm. The catalyst-containing MG solutions were stirred in the dark for 60 min. MG adsorption by the composites containing different metal oxides is shown in Fig. 6.

As can be seen in this figure, the LTF composite catalyst shows greater adsorption ability than the other catalysts. This observation is in complete agreement with the results for the surface area of the catalysts (Table 1). The adsorption results clearly show that increasing the pH of the solution increases the ability of this catalyst to adsorb malachite green. According to the physical nature of surface adsorption, the reasons for this observation can be attributed to the surface properties of the LTF catalyst compared to other prepared catalysts (Table 1 and Fig. 4), the negative charge on the surface of the catalyst, the presence of hydroxyl species on the surface and the formation of hydrogen bonds (Hojjati-Najafabadi et al. 2023).
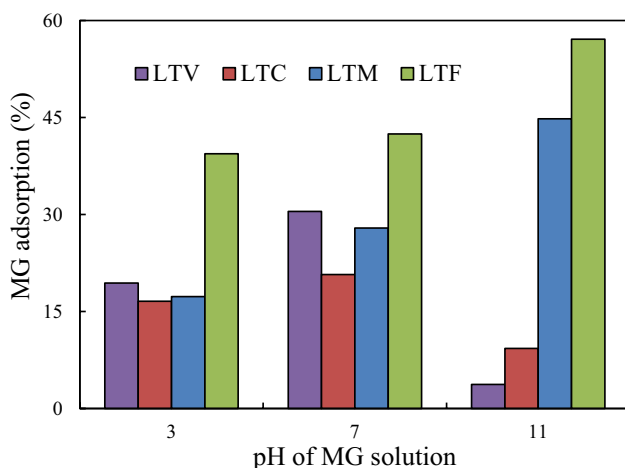

Fig. 6 MG dye adsorption by different composite catalysts as a function of pH of the dye solution

The surface charge and electrostatic interactions have an influence on the adsorption of MG. One of the factors influencing the surface charge is the pH of the solution. For this reason, the effect of a pH change on the performance of catalysts in the range of 3–11 was investigated. As mentioned above, by an increase in pH, the adsorption of MG also increased with the increase in pH, from 39% at pH 3 to 57% at pH 11 for the LTF catalyst. The reason for this observation can be explained by the cationic nature of MG and its tendency to interact with positively charged surfaces, which is possible in an alkaline solution (Hojjati-Najafabadi et al. 2023). The surface charge of a catalyst plays a crucial role in determining its adsorption capacity for various substances, including dyes. At high pH levels, the surface of many catalysts, particularly those composed of metal oxides, can acquire a net positive charge. This phenomenon is related to the concept of the isoelectric point (IEP) and the point of zero charge (PZC) of the material. The IEP is the pH at which the material carries no net electrical charge, meaning the positive and negative charges on the surface balance out. Below the IEP, the material tends to have a net positive charge, while above it, the material tends to have a net negative charge. The PZC, on the other hand, is the pH at which the surface of the material has no net charge due to the absence of specifically adsorbed positive or negative charges. This means that at the PZC, the surface is neither attracting nor repelling ions from the solution.

In the context of our study, the catalyst surface becomes positively charged at high pH levels because the pH exceeds the IEP of the catalyst material. This positive charge allows for effective interaction and adsorption of the cationic MG dye, which also carries a positive charge under these conditions. This interaction is facilitated by the electrostatic attraction between the positively charged catalyst surface and the cationic dye molecules (Parsafard et al. 2024). The adsorption of MG via LTV and LTC does not seem to be favorable at pH 11. Here, electrostatic interactions are probably not effective, but the hydrophobic–hydrophilic interactions or hydrogen bonding in an acidic solution are effective (Tran et al. 2022).

After evaluating the adsorption–desorption equilibrium in a dark environment, the photo-decolorization efficiency (PDE) of MG on the synthesized catalysts was studied under UV and visible light for 35 min. The results obtained under UV and visible light are shown in Figs. 7 and 8, respectively. As can be seen from these figures, the range of changes in PDE under UV and visible light at different pH values is as follows:

Under UV light:

$$pH = 3 : 1.02 \leq PDE(\%) \leq 56.99$$

pH = 7 : 0.91 ≤ PDE(%) ≤ 33.76

pH = 11 : 6.18 ≤ PDE(%) ≤ 57.07

Under Vis light:

pH = 3 : 1.26 ≤ PDE(%) ≤ 62.27

pH = 7 : 0.66 ≤ PDE(%) ≤ 54.09

pH = 11 : 0.7 ≤ PDE(%) ≤ 78.62

According to the obtained results, the LTM catalyst has on average the highest dye degradation efficiency under UV irradiation at different pH values (Fig. 7), while a much higher efficiency with visible light (Fig. 8) was obtained for the LTF catalyst under similar conditions. The best performance of these catalysts is also obtained at alkaline pH

values. As can be seen, the PDE of the MG dye increased sharply with time up to 35 min.

The observed sequences of photocatalytic performance under the influence of visible and ultraviolet light and also at different pH values are as follows:

Under UV light: LTM > LTC > LTF > LTV.
Under visible light: LTF > LTV > LTC > LTM.
pH of solution under UV–Vis light: 11 > 3 > 7.
Several reasons can be cited for these observations:

– In general, it can be said that the photocatalytic activity of LTF catalyst is higher than others under different used conditions. The high photocatalytic activity of this catalyst could be related to the small particle size and larger surface area (Table 1). In the explanation of this observation, it should be said that photoabsorption refers to the ability of a material to absorb photons and promote electrons from the valence band to the conduction band,
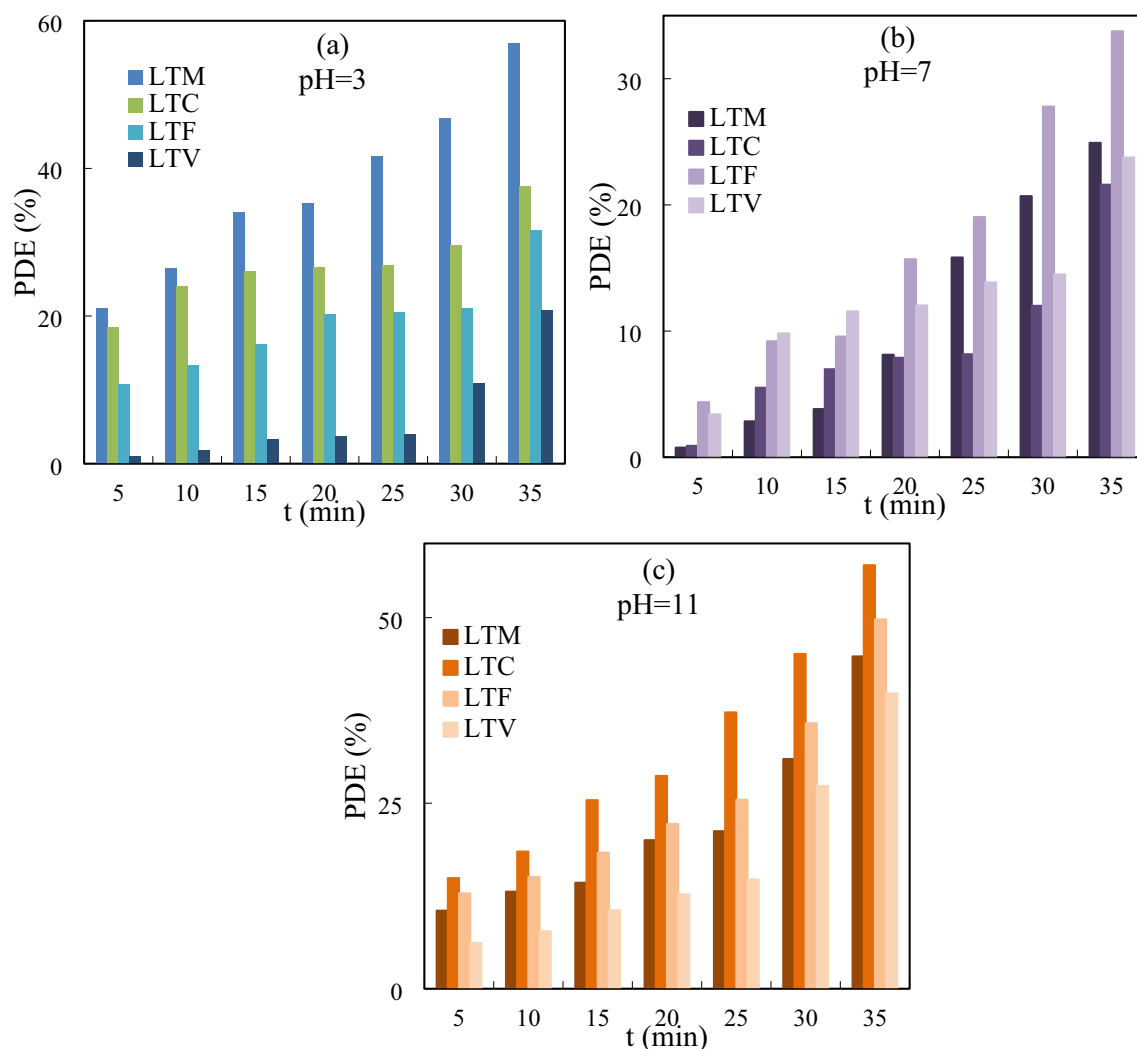

Fig. 7 PDE of MG dye by different composite catalysts as a function of process time at **a** pH = 3, **b** pH = 7 and **c** pH = 11 under UV light
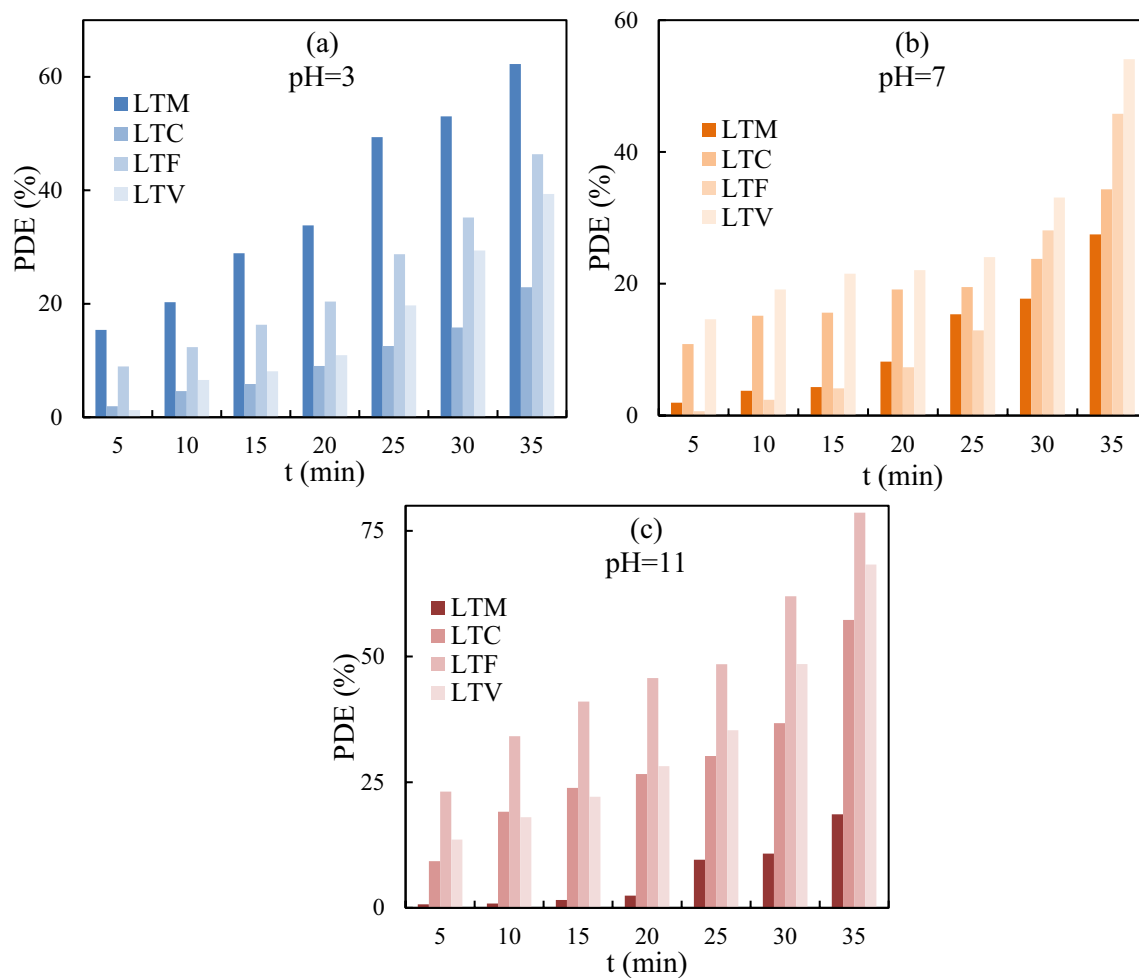
Fig. 8 PDE of MG dye by different composite catalysts compared to process time at **a** pH = 3, **b** pH = 7 and **c** pH = 11 under visible light

creating electron–hole pairs. These pairs are responsible for initiating redox reactions in photocatalysis. The efficiency of this process is influenced by several factors, including the particle size of the photocatalyst. Smaller particle sizes generally offer a larger surface area and more active sites for photoabsorption, potentially enhancing the photocatalytic activity. However, smaller particles can also lead to increased recombination rates of the photo-generated electron–hole pairs, which can diminish the overall photocatalytic efficiency. This trade-off between increased surface area and potential for higher recombination rates is a complex aspect of photocatalyst design. Moreover, the morphology and surface chemistry of the photocatalyst play significant roles in its photocatalytic performance. Surface defects and functional groups can act as traps for charge carriers, affecting their mobility and availability for redox reactions. The presence of these defects and groups can influence the photocatalyst's ability to absorb light efficiently and facilitate charge separation, thus impacting its photocatalytic activity. In our case, the high photocatalytic activity of the catalyst could indeed be attributed to a combination of factors, including its small particle size, larger surface area and possibly efficient photoabsorption capabilities.

- According to a published report by Asiltürk and coworkers (Asiltürk et al. 2009), TiO_2 undergoes intrinsic excitation under UV light irradiation. This is the case when the presence of iron ions in the catalytic structure causes the electronic transition from the doping energy level to the conduction band of TiO_2 under visible light. It can be concluded that the increase in PDE for the LTF catalyst is due to the shift of photocatalytic activity to the visible region in addition to the UV region due to the presence of TiO_2.

Model fitting and statistical analysis

The experimental matrix proposed by CCD for the photo-degradation of MG is shown in Table S1. The empirical

Table 2 ANOVA results for the quadratic model

Source	Sum of squares	df	Mean square	F-value	p-value
Model (significant)	8907.70	5	1781.54	2700.82	$<10^{-4}$
A-pH	1214.53	1	1214.53	1841.23	$<10^{-4}$
B-t	4240.17	1	4240.17	6428.11	$<10^{-4}$
AB	81.74	1	81.74	123.92	$<10^{-4}$
A2	2273.93	1	2273.93	3447.28	$<10^{-4}$
B2	1200.22	1	1200.22	1819.53	$<10^{-4}$
Residual	4.62	7	0.66		
Lack-of-fit	4.62	3	1.54		
Pure error	0.00	4	0.00		
Cor. total	8912.32	12			
R^2	0.9995		Std. Dev	0.81	
Adjusted R^2	0.9991		Mean	26.77	
Predicted R^2	0.9962		C.V. %	3.03	
Adeq. precision	142.83				

relationships between the independent variables and the response are a second-order polynomial equation:

$$MOPDE = +44.74 - 14.22pH - 1.40t \\ + 0.08pH * t + 1.13pH^2 + 0.06t^2 \tag{3}$$

The adequacy of this empirical second-order polynomial model (Table 2) was tested by analysis of variance (ANOVA). The F-value for the model is 2700.82, which means that this model is highly significant. There is only a 0.01% chance that such a large F-value could occur due to noise. The *p*-value for this model is $<10^{-4}$, which also means that the model is significant (Parsafard 2023).

The "lack-of-fit" of 4.62 shows that this parameter is not significant in relation to the pure error and confirms the good predictability of the model (Parsafard 2023).

The predicted R^2 of 0.9962 agrees well with the adjusted R^2 of 0.9991, confirming the good predictability of the model (Fig. S1).

The Adeq. precision of 142.831 indicates a reasonable signal, so this model can be used to navigate the design space. The independent variables, including pH (A) and process time (B), are highly significant parameters with $p < 10^{-4}$. In addition, the second-order effects of these parameters and their dual interaction are significant at $p < 10^{-4}$ (Parsafard 2023).

The negative coefficients of the quadratic terms in the polynomial expression (Eq. 3) indicate their negative influence on the photocatalytic degradation of MG. To better understand of the interactions between these variables, 3D surface plots were presented in Fig. S2. The results of the interactions between these two independent variables

and the response show that the efficiency of photocatalytic degradation of MG increases with increasing process time and pH value. This can be attributed to the surface charge properties of the photocatalyst. The desirability function was used to determine the optimal conditions for MG degradation. Since the main objective for this study is to achieve higher photodegradation efficiency, the optimum conditions for maximum MG photodegradation efficiency (78.62%) were found at a pH value of 11 and a process time of 35 min (Fig. S3) (Parsafard 2023).

Conclusion

In this study, the successful preparation of La@M_xO_y-TiO$_2$ composite catalysts was investigated using the sol–gel method. Among the prepared catalysts, the Fe$_2$O$_3$/TiO$_2$ composite showed the most effective adsorption and photodegradation efficiency for malachite green. The high adsorption of this composite is mainly due to its large surface area and textural properties. The experimental design methodology was used to optimize the parameters for the photocatalytic degradation of malachite green using La@M_xO_y-TiO$_2$ composite catalysts. The relationship between the photodegradation efficiency of malachite green and two independent variables: pH and process time were predicted by a quadratic model. Under the optimized conditions of pH 11 and process time of 35 min, the degradation efficiency of MG reached 78.62% over La@ Fe$_2$O$_3$/TiO$_2$. The regression analysis with an R^2 value of 0.9995 showed a good agreement between the experimental results and the predicted values.

Declarations

References

Abbas N, Shao GN, Haider MS, Imran SM, Park SS, Kim HT (2016) Sol–gel synthesis of TiO_2-Fe_2O_3 systems: Effects of Fe_2O_3 content and their photocatalytic properties. J Ind Eng Chem 39:112–120. https://doi.org/10.1016/j.jiec.2016.05.015

Almontasser A, Parveen A (2020) Preparation and characterization of chromium oxide nanoparticles. AIP Conf Proc 2220:020010. https://doi.org/10.1063/5.0001685

Asiltürk M, Sayılkan F, Arpaç E (2009) Effect of Fe^{3+} ion doping to TiO_2 on the photocatalytic degradation of Malachite green dye under UV and vis-irradiation. J Photochem Photobiol 203(1):64–71. https://doi.org/10.1016/j.jphotochem.2008.12.021

Balakrishnan A, Appunni S, Chinthala M, Vo DVN (2022) Biopolymer-supported TiO2 as a sustainable photocatalyst for wastewater treatment: a review. Env Chem Let 20(5):3071–3098. https://doi.org/10.1007/s10311-022-01443-8

Bibi S, Ahmad A, Anjum MAR, Haleem A, Siddiq M, Shah SS, Al Kahtani A (2021) Photocatalytic degradation of malachite green and methylene blue over reduced graphene oxide (rGO) based metal oxides (rGO-Fe_3O_4/TiO_2) nanocomposite under UV-visible light irradiation. J Environ Chem Eng 9(4):105580. https://doi.org/10.1016/j.jece.2021.105580

Bootluck W, Chittrakarn T, Techato K, Jutaporn P, Khongnakorn W (2022) S-scheme α-Fe_2O_3/TiO_2 photocatalyst with Pd cocatalyst for enhanced photocatalytic H_2 production activity and stability. Catal Let. https://doi.org/10.1007/s10562-021-03873-5

Chakraborty J, Nath I, Verpoort F (2022) A physicochemical introspection of porous organic polymer photocatalysts for wastewater treatment. Chem Soc Rev 51(3):1124–1138. https://doi.org/10.1039/D1CS00916H

Farahmandjou M, Abaeiyan N (2017) Chemical synthesis of vanadium oxide (V_2O_5) nanoparticles prepared by sodium metavanadate. J Nanomed Res 5(1):00103. https://doi.org/10.15406/jnmr.2017.05.00103

Farzaneh F, Najafi M (2011) Synthesis and characterization of Cr_2O_3 nanoparticles with triethanolamine in water under microwave irradiation. J Sci I R 22(4):329–333

Fatima R, Warsi MF, Zulfiqar S, Ragab SA, Shakir I, Sarwar MI (2020) Nanocrystalline transition metal oxides and their composites with reduced graphene oxide and carbon nanotubes for photocatalytic applications. Ceram Int 46(10):16480–16492. https://doi.org/10.1016/j.ceramint.2020.03.213

Giang NTH, Hai ND, Thinh NT, Tan NN, Phuong LP, Thinh DB, Van Duc N, Dai Viet VN, Duy HK, Phong MT, Hieu NH (2022) Enhanced photocatalytic degradation of malachite green by sulfur-doped titanium dioxide/porous reduced graphene oxide. Diam Relat Mater 129:109321. https://doi.org/10.1016/j.diamond.2022.109321

Hojjati-Najafabadi A, Esfahani PN, Davar F, Aminabhavi TM, Vasseghian Y (2023) Adsorptive removal of malachite green using novel GO@ZnO-$NiFe_2O_4$-$αAl_2O_3$ nanocomposites. Chem Eng J 471:144485. https://doi.org/10.1016/j.cej.2023.144485

Huang Y, Cao JJ, Kang F, You SJ, Chang CW, Wang YF (2017) High selectivity of visible-light-driven La-doped TiO_2 photocatalysts for NO removal. Aerosol Air Qual Res 17(10):2555–2565

Jaffari ZH, Abbas A, Lam SM, Park S, Chon K, Kim ES, Cho KH (2023) Machine learning approaches to predict the photocatalytic performance of bismuth ferrite-based materials in the removal of malachite green. J Hazard Mater 442:130031. https://doi.org/10.1016/j.jhazmat.2022.130031

Kallawar GA, Bhanvase BA, Sathe BR (2023) Sonochemically prepared bismuth doped titanium oxide-reduced graphene oxide (Bi@TiO_2-rGO) nanocomposites for effective visible light photocatalytic degradation of malachite green. Diam Relat Mater 139:110423. https://doi.org/10.1016/j.diamond.2023.110423

Khurshid F, Jeyavelan M, Nagarajan S (2021) Photocatalytic dye degradation by graphene oxide doped transition metal catalysts. Synth Met 278:116832. https://doi.org/10.1016/j.synthmet.2021.116832

Lam SM, Sin JC, Satoshi I, Abdullah AZ, Mohamed AR (2014a) Significantly improved sunlight photocatalytic activity via Nb_2O_5/ZnO nanorod composites and the mechanism study. Appl Catal a: Gen 471:126–135. https://doi.org/10.1016/j.apcata.2013.12.001

Lam SM, Sin JC, Abdullah AZ, Mohamed AR (2014b) Transition metal oxide loaded ZnO nanorods: preparation, characterization and their UV–vis photocatalytic activities. Sep Pur Tech 132:378–387. https://doi.org/10.1016/j.seppur.2014.05.043

Pan Q, Li A, Zhang Y, Yang Y, Cheng C (2020) Rational design of 3D hierarchical ternary SnO_2/TiO_2/$BiVO_4$ arrays photoanode toward efficient photoelectrochemical performance. Adv Sci 7(3):1902235. https://doi.org/10.1002/advs.201902235

Parsafard N (2023) Optimization of main parameters affecting activity and octane number produced from catalytic isomerization of n-heptane using response surface methodology. Iran J Catal 13(2):125–133. https://doi.org/10.30495/IJC.2023.1980650.1994

Parsafard N, Abedi R, Moodi H (2024) Ternary tin-doped titanium dioxide/calcium oxide (Sn-TiO_2/CaO) composite as a photocatalyst for efficient removal of toxic dyes. RSC Adv 14(28):19984–19995. https://doi.org/10.1039/D4RA03641G

Pei CC, Woon WFL (2013) Photocatalytic degradation of Rhodamine B by TiO_2/ZnO nanofibers under visible-light irradiation. Sep Purif Technol 114:108–116. https://doi.org/10.1016/j.seppur.2013.04.032

Rauf MA, Meetani MA, Hisaindee S (2011) An overview on the photocatalytic degradation of azo dyes in the presence of TiO_2 doped with selective transition metals. Desalination 276(1–3):13–27. https://doi.org/10.1016/j.desal.2011.03.071

Sharma J, Sharma S, Soni V (2023) Toxicity of malachite green on plants and its phytoremediation: a review. Reg Stud Mar Sci 62:102911. https://doi.org/10.1016/j.rsma.2023.102911

Taylor RP, Schrader GL (1991) Lanthanum catalysts for methane oxidative coupling: a comparison of the reactivity of phases. Ind Eng Chem Res 30(5):1016–1023. https://doi.org/10.1021/ie00053a025

Van Tran T, Nguyen DTC, Kumar PS, Din ATM, Qazaq AS, Vo DVN (2022) Green synthesis of Mn_3O_4 nanoparticles using Costus woodsonii flowers extract for effective removal of malachite green dye. Environ Res 214:113925. https://doi.org/10.1016/j.envres.2022.113925

Verma A, Thakur S, Mamba G, Gupta RK, Thakur P, Thakur VK (2020) Graphite modified sodium alginate hydrogel composite for efficient removal of malachite green dye. Int J Biol Macromol 148:1130–1139. https://doi.org/10.1016/j.ijbiomac.2020.01.142

Warsi MF, Shaheen N, Sarwar MI, Agboola PO, Shakir I, Zulfiqar S (2021) A comparative study on photocatalytic activities of various transition metal oxides nanoparticles synthesized by wet chemical route. Desalinat Water Treat 211:181–195. https://doi.org/10.5004/dwt.2021.26463

Wu DZ, Fan XM, Dai J, Liu HR, Liu H, Zhang FZ (2012) Preparation and photocatalytic properties of Cu_2S/tetrapod-like ZnO whisker nanocomposites. Chin J Catal 33:802–807. https://doi.org/10.1016/S1872-2067(11)60380-X

Yulizar Y, Abdullah I, Surya RM, Alifa NL (2023) Green synthesis of novel $YMnO_3$-doped TiO_2 for enhanced visible-light-driven photocatalytic degradation of malachite green. J Environ Manage 342:118139. https://doi.org/10.1016/j.jenvman.2023.118139

Zhang JY, Boyd IW, O'sullivan BJ, Hurley PK, Kelly PV, Senateur JP (2002) Nanocrystalline TiO_2 films studied by optical, XRD and FTIR spectroscopy. J Non Cryst Solids 303(1):134–138. https://doi.org/10.1016/S0022-3093(02)00973-0

Zhang M, Liang X, Liu Y (2024) Co-CNT/TiO_2 composites effectively improved the photocatalytic degradation of malachite green. Ion 30:521–527. https://doi.org/10.1007/s11581-023-05339-7